

Cite this: *Dalton Trans.*, 2022, **51**,
3636

Activating the oxygen electrocatalytic activity of layer-structured $\text{Ca}_{0.5}\text{CoO}_2$ nanofibers by iron doping†

Mingyu Li,^{a,b,c} Bote Zhao,^{id} *^{c,d} Yun Zhao,^d Yu Chen,^{id} ^d and Meilin Liu,^{id} *^c

The development of low-cost, highly efficient and stable electrocatalysts for the oxygen evolution reaction (OER) is of great significance for many promising energy storage and conversion applications, including metal–air batteries and water splitting technology. Here we report a layer-structured $\text{Ca}_{0.5}\text{CoO}_2$ nanofibers composed of interconnected ultrathin nanoplates, synthesized using an electrospinning process. The OER activity of $\text{Ca}_{0.5}\text{CoO}_2$ can be dramatically improved by iron doping, and the overpotential of $\text{Ca}_{0.5}\text{Co}_{1-x}\text{Fe}_x\text{O}_2$ ($x = 0.25$) is only 346 mV at a current density of 10 mA cm⁻². The mass activity and intrinsic activity of $\text{Ca}_{0.5}\text{Co}_{0.75}\text{Fe}_{0.25}\text{O}_2$ at 1.6 V are, respectively, ~18.7 and ~11.4 times higher than those of $\text{Ca}_{0.5}\text{CoO}_2$. Iron doping modifies the electronic structure of $\text{Ca}_{0.5}\text{CoO}_2$, resulting in partial oxidation of the surface cobalt and increased amount of highly oxidative species ($\text{O}_2^{2-}/\text{O}_2$). Consequently, $\text{Ca}_{0.5}\text{Co}_{0.75}\text{Fe}_{0.25}\text{O}_2$ nanofibers with tuned electronic states have shown great potential as cost-effective and efficient electrocatalysts for OER.

Received 16th November 2021.

Accepted 18th January 2022

DOI: 10.1039/d1dt03883d

rsc.li/dalton

1. Introduction

Developing renewable energy is essential to mitigate the growing concern of the energy crisis worldwide.^{1–4} However, the practical application of the storage and conversion for sustainable alternatives is often limited by sluggish chemical reactions.^{5,6} In particular, the bottleneck of hydrogen production in water splitting is the kinetically sluggish oxygen evolution reaction (OER).^{7,8} The noble metal oxides IrO_2 and RuO_2 are currently the superior electrocatalysts for the OER but their widespread applications are severely limited by their resource deficiency and the noble metal dissolution at high potential.^{9–11} Therefore, rational design of low-cost, efficient and durable alternatives is of great significance but remains a large challenge facing the sustainable energy application field.

In the past decade, 3d transition metal-based layer-structured materials have drawn increasing attention as alternative candidates for the OER due to their resource abundance and

competitive OER activity in comparison to noble IrO_2 and RuO_2 .^{12,13} In particular, a series of LiCoO_2 -based electrocatalysts has been explored for oxygen electrocatalysis. For instance, $\text{Li}_{0.5}\text{CoO}_2$ was designed as an efficient catalyst for the OER.¹⁴ A LiCoO_2 -based electrocatalyst was also developed by a combination of Mg doping and a shear force-assisted exfoliation strategy.¹⁵ Further, it has been demonstrated that the introduction of La breaks the O_h symmetry of the CoO_6 octahedron in LiCoO_2 , which results in enhanced oxygen evolution activity.¹⁶ However, LiCoO_2 as a catalyst suffers from low abundance, high cost, low activity and Li^+ dissociation. In contrast to lithium, calcium, with a larger ionic radius, is relatively abundant in the Earth's crust (3rd most abundant metallic element).¹⁷ Thus, $\text{Ca}_{0.5}\text{CoO}_2$ could be a low-cost alternative to layer-structured LiCoO_2 . Nevertheless, in comparison with LiCoO_2 , Ca-containing layered oxides have been rarely reported as electrocatalysts for the OER.

Cation doping has been proven to be a promising technique for the modification of transition metal-based electrocatalysts to improve their electrocatalytic activity.¹⁸ In particular, Fe cations have been found to be effective dopants to enhance OER activities of transition metal-based catalysts.¹⁹ For instance, the electrocatalytic activities of Ni_2P could be effectively improved by the introduction of iron species, indicating the superior iron species-modified electrochemical performance.²⁰ Fe-doping was also found to be conducive to optimize the electronic conductivity of NiSe_2 and create more active sites due to heteroatom displacement defects.²¹ Fe-doped $\text{Ni}(\text{OH})_2$ nanosheets prepared by a cation exchange process

^aKey Laboratory of Groundwater Resources and Environment, Ministry of Education, Jilin University, Changchun, 130021 Jilin, China

^bJilin Provincial Key Laboratory of Water Resources and Environment, Jilin University, Changchun 130021, Jilin, China

^cSchool of Materials Science and Engineering, Georgia Institute of Technology, Atlanta, GA 30332-0245, USA. E-mail: botezhao@scut.edu.cn, meilin.liu@mse.gatech.edu

^dSchool of Environment and Energy, South China University of Technology, Guangzhou 510006, China

† Electronic supplementary information (ESI) available. See DOI: 10.1039/d1dt03883d

demonstrated improved catalytic performance compared with pristine Ni(OH)₂, which was attributed to the higher electrochemical active surface area and enhanced surface wettability.²²

In addition to cation doping,^{21,23,24} nanostructure engineering is an effective strategy to enhance the mass activity of catalysts by increasing the exposed electrocatalytic active sites.²⁵ The combination of composition tuning and nanostructure engineering is expected to result in significantly enhanced electrocatalytic activity.^{26,27}

Herein, we have successfully designed layer-structured Ca_{0.5}CoO₂ (denoted as CC) nanofibers composed of interconnected ultrathin nanoplates using an electrospinning process. The intrinsic activity and mass activity have been enhanced dramatically with nanostructure engineering and iron doping.^{28,29} Iron doping modifies the electronic structure of CC through partial oxidation of the surface Co³⁺ and the increase of highly reactive oxygen species (O₂²⁻/O₂). In addition, based on the unique nanofiber structure, a high surface area has been achieved with more active sites exposed. These findings endow the active and robust Ca_{0.5}Co_{0.75}Fe_{0.25}O₂ with potential as a superior electrocatalyst for the OER.

2. Experimental section

2.1. Catalyst synthesis

CC and Ca_{0.5}Co_{1-x}Fe_xO₂ (CCFx) nanofibers were synthesized by an electrospinning method followed by an annealing process ($x = 0.063, 0.125$ and 0.25 , denoted as CCF0.063, CCF0.125 and CCF0.25, respectively). In a typical process, stoichiometric amounts of Ca(NO₃)₂·4H₂O and Co(NO₃)₂·6H₂O were dissolved in *N,N*-dimethylformamide (DMF, 5 mL). After stirring at room temperature for 30 min, PVP powder (1.3 g) and ethanol (5 mL) were added to the above solution, which was further stirred overnight to obtain a uniform precursor solution. The as-prepared solution was transferred into a plastic syringe for electrospinning. The parameters for the electrospinning were as follows: a 27-G needle, a feeding rate of 0.3 mL min⁻¹, an applied voltage of 18 kV, a needle tip to drum collector distance of 15 cm and a relative humidity of 25%–35%. The as-obtained electrospun nanofibers were annealed in air at 650 °C for 3 h with heating and cooling rates of 1 °C min⁻¹ and 3 °C min⁻¹, respectively.

2.2. Material characterization

X-ray diffraction (XRD) patterns were collected with an X'Pert PRO Alpha-1 X-ray diffractometer. The morphologies of the as-prepared catalysts were characterized by scanning electron microscopy (SEM, SU8010, Hitachi) and high-resolution transmission electron microscopy (HRTEM, FEI Tecnai G² F30). X-ray photoelectron spectroscopy (XPS) measurements were carried out on a Thermo K-Alpha XPS spectrometer equipped with a monochromatic Al-K α X-ray source ($h\nu = 1468.6$ eV).

2.3. Electrochemical measurement

The catalyst ink was obtained by mixing the catalyst (2.0 mg), acetylene black carbon (0.5 mg), Nafion solution (25.0 μ L) and deionized water/isopropanol solvent (3 : 1 (v/v), 1 mL). Before drop-casting, the catalyst ink was sonicated for 1 h to obtain a uniform solution. The ink solution (20 μ L) was dropped on a glassy carbon (GC, 5 mm in diameter) electrode and fully dried before conducting measurements. The mass loading of the sample was 0.202 mg cm⁻². A conventional three electrode cell system was employed using a GC electrode as the working electrode, a Pt wire as the counter electrode, an Hg/HgO electrode as the reference electrode and KOH aqueous solution (1 M) as the electrolyte. The electrode was saturated with oxygen before the measurements were conducted. Electrochemical measurements were obtained on a Solartron electrochemical workstation equipped with a rotating disk electrode (RDE) system (Pine Instrument Company, USA).

To evaluate the OER activity, linear sweep voltammetry (LSV) curves were plotted from 0.3 to 0.73 V vs. Hg/HgO at a scan rate of 10 mV s⁻¹ with a rotation rate of 1600 r min⁻¹. Tafel plots were obtained from the steady-state measurements. Electrochemical impedance spectroscopy (EIS) measurements were collected from 100 kHz to 50 mHz at a potential of 0.65 V vs. Hg/HgO with 10 mV amplitude. Chronopotentiometric measurements were recorded on the working electrode at a current density of 10 mA cm⁻² for 12 h. All potentials were calibrated with a reversible hydrogen electrode (RHE) and corrected with *i*R-compensation.

3. Results and discussion

The layer-structured CC nanofibers were synthesized by an electrospinning method (Fig. 1). Fe-doped CC nanofibers (*i.e.*, Ca_{0.5}Co_{1-x}Fe_xO₂, denoted as CCFx, $x = 0.063, 0.125, 0.25$ and 0.375) were also prepared in the same fashion.

Fig. 2 shows the SEM images of CCF. All CCF samples doped with different amounts of iron are nanofibers with average diameters of *ca.* 70 nm (Fig. S1[†]). Specifically, Ca_{0.5}CoO₂ and Ca_{0.5}Co_{0.937}Fe_{0.063}O₂ have nanofiber architecture composed of interconnected nanoplates. With increasing the amounts of doped iron to $x = 0.125$ and 0.25 , the morphologies of Ca_{0.5}Co_{0.875}Fe_{0.125}O₂ and Ca_{0.5}Co_{0.75}Fe_{0.25}O₂ are still nanofiber structures but appear to be composed of nanoparticles (Fig. 2c and d). Elemental mapping shown in Fig. S2[†] demonstrates the uniform distribution of Ca, Co, Fe and O elements (Table S1[†]).

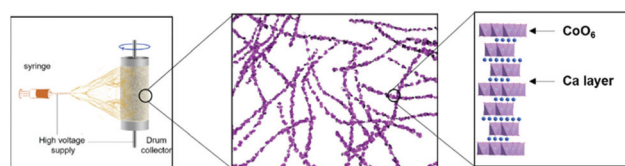


Fig. 1 Schematic illustration for the preparation of CC nanofibers.

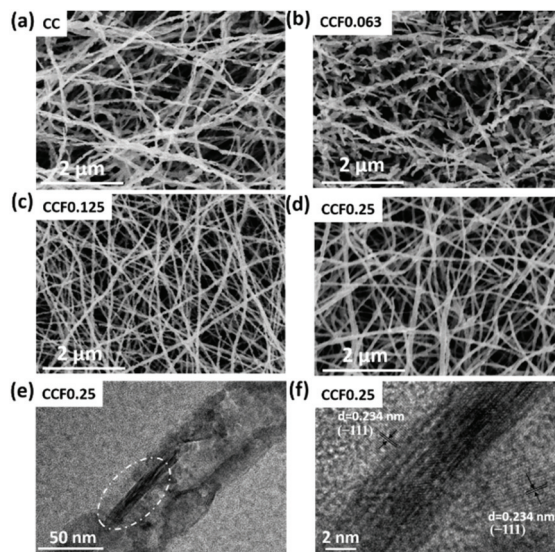


Fig. 2 (a–d) SEM images of (a) CC, (b) CCF0.063, (c) CCF0.125 and (d) CCF0.25. (e) TEM and (f) HRTEM images of CCF0.25.

The TEM analysis indicates that CCF0.25 has discontinuous pores inside (Fig. 2e and S3†), which were created by the gases released from the decomposition of the metal nitrate precursors and PVP. The lattice spacing of CCF0.25 was measured to be 0.234 nm by HRTEM (Fig. 2f), which corresponds to the (−111) facet of the CaCo_2O_4 crystal, and the HRTEM results are consistent with the XRD patterns. The Brunauer–Emmett–Teller (BET) surface areas are 22.3, 20.8, 31.3 and 35.3 $\text{m}^2 \text{g}^{-1}$ for CC, CCF0.063, CCF0.125 and CCF0.25, respectively (Fig. S4†).

Fig. 3 illustrates the XRD patterns of the as-obtained CC and CCF x nanofibers doped with different amounts of iron. Among the samples, the diffraction peaks of the as-synthesized CC and CCF0.063 were in accordance with the standard patterns of layer-structured CaCo_2O_4 (JCPDS No. 51-1760). With further increasing the iron content of CCF x to $x = 0.125$ and 0.25, some of the diffraction peaks disappeared but no impur-

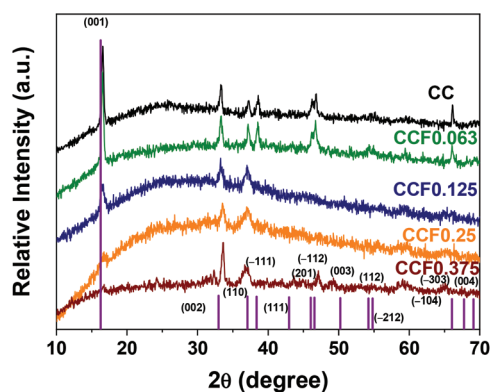


Fig. 3 XRD patterns of CC, CCF0.063, CCF0.125, CCF0.25 and CCF0.375.

ity phase was detected. The full width at half maximum (FWHM) of typical peaks increased and the peak intensity decreased, which could be attributed to the presence of disordered structures. However, the phase of CaFe_2O_5 (JCPDS No. 38-0408) emerged in the pattern of the CCF0.375 sample, indicating that the amount of iron doping in the cobalt site should be less than 0.375. Moreover, the XRD results are in accordance with those of the SEM images. Specifically, CC and CCF0.063 had nanofiber architecture composed of interconnected nanoplates. With increasing the amounts of doped iron to $x = 0.125$ and 0.25, the morphologies of CCF0.125 and CCF0.25 were still nanofiber structures, but the interconnected nanoplates became smaller (Fig. 2c and d).

The OER performance of the as-prepared catalysts was measured with a rotating disk electrode (RDE) system. The catalyst was uniformly drop-casted on a GC RDE with an areal mass loading of 0.202 mg cm^{-2} for all samples. The typical iR-corrected OER LSV curves are shown in Fig. 4a and Fig. S5.† The CCF0.25 nanofibers exhibit the lowest onset potential and overpotential (346 mV) at 10 $\text{mA cm}^{-2}_{\text{geo}}$. The overpotential of the CCF0.25 nanofibers was much lower than that of the CC sample (410 mV) at the same current density. Additionally, the turnover frequency values of CC, CCF0.063, CCF0.125 and CCF0.25 were calculated to be $6.0 \times 10^{-4} \text{ s}^{-1}$, $1.2 \times 10^{-3} \text{ s}^{-1}$, $3.0 \times 10^{-3} \text{ s}^{-1}$ and 0.02 s^{-1} , respectively (Table S1†). Moreover, the continuous cyclic voltammetry (CV) measurements exhibit that the initial activation of all CC and CCF x electrocatalysts was done after 15 cycles (Fig. S6†).

Tafel plots were constructed from the steady-state measurements, and the Tafel slope of CCF0.25 is the lowest (39.3 mV dec^{-1}) among the electrocatalysts, indicating that the OER performance and kinetics are co-enhanced by iron doping (Fig. 4b). EIS measurements were recorded to obtain the charge transfer resistance (R_{ct}) of the electrocatalysts (Fig. 4c).

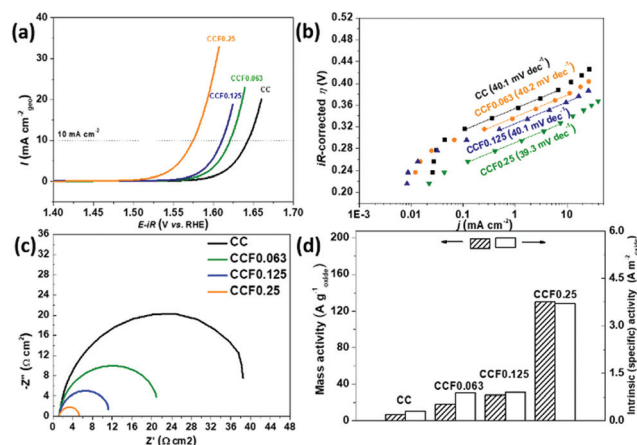


Fig. 4 (a) iR-corrected OER LSV curves of CC, CCF0.063, CCF0.125 and CCF0.25 nanofibers. (b) Tafel plots obtained by the steady-state measurements. (c) Electrochemical impedance spectra recorded at a constant potential of 1.566 V (vs. RHE). (d) Mass activities and intrinsic activities of the electrocatalysts at 1.6 V.

The R_{ct} of CCF0.25 is much smaller than that of CC, CCF0.063 and CCF0.125, indicating the fastest charge transfer capability of CCF0.25 during the OER process. Moreover, the mass loading-normalized current density (mass activity) of CCF0.25 at 1.6 V (vs. RHE) is *ca.* 18.7, 6.2 and 3.6 times higher than that of CC, CCF0.063 and CCF0.125, respectively. The BET surface area-normalized current density (intrinsic activity) of CCF0.25 at 1.6 V (vs. RHE) is *ca.* 11.4, 3.2 and 3.1 times higher than that of CC, CCF0.063 and CCF0.125, respectively (Fig. 4d). The detailed electrocatalytic parameters of the catalysts are summarized in Table S2.† Compared with recently reported electrocatalysts, CCF0.25 nanofibers show comparable OER activity in terms of *iR*-corrected overpotential, Tafel slope and mass loading in 1 M KOH, suggesting that the CCF0.25 nanofiber is a highly promising electrocatalyst for OER (Table S3†).

The stability of CCF0.25 was measured by chronopotentiometry. There are no significant changes in the potential (from 1.57 to 1.58 V) of the CCF0.25 catalyst after testing at a current density of 10 mA cm⁻²_{geo} for 12 h (Fig. 5a). The morphology and structure of CCF0.25 after the stability test were also investigated. The electrocatalysts still maintain their nanofiber structure (Fig. S7†). The HRTEM image further shows that CCF0.25 nanofibers after the stability test still possess a lattice spacing of 0.234 nm, which is in agreement with the (-111) facet of the CaCo₂O₄ crystal (Fig. 5b). The HRTEM results are consistent with the results of the as-prepared samples (Fig. 2e and f).

XPS characterization was further carried out to explore the information of the surface electronic states in the CC and CCF nanofibers (Fig. 6). Both the XPS survey spectra of CC and CCF0.25 (Fig. 6a) confirm the existence of Ca, Co and O. However, there is difference in the peaks from 710 eV to 720 eV, which correspond to Co Auger in CC and Fe 2p in CCF0.25, respectively. High-resolution Co 2p XPS spectra were also measured in the CC and CCF0.25 samples (Fig. 6b). Compared with CC, a lower satellite (sat) peak was observed in CCF0.25. A higher binding energy of the main peak was observed in the Co 2p spectra, indicating the partial oxidation of surface Co in CCF0.25 (Fig. S8†). The Co 2p_{3/2} peak of the as-prepared CC and CCF0.25 catalyst indicates that Co exists mainly in the form of octahedral Co³⁺ (779.6 eV) with a minor portion of tetrahedral Co²⁺ (781.2 eV), and the amount of Co³⁺ has been

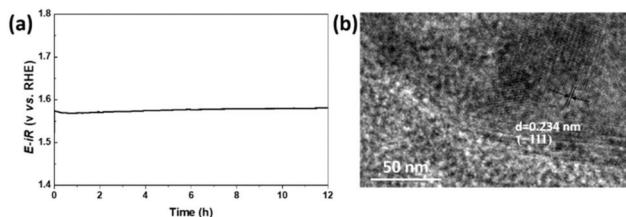


Fig. 5 (a) *iR*-corrected chronopotentiometry curve of CCF0.25 nanofibers at a constant current density of 10 mA cm⁻²_{geo}. (b) HRTEM image of CCF0.25 after a stability test for 12 h.

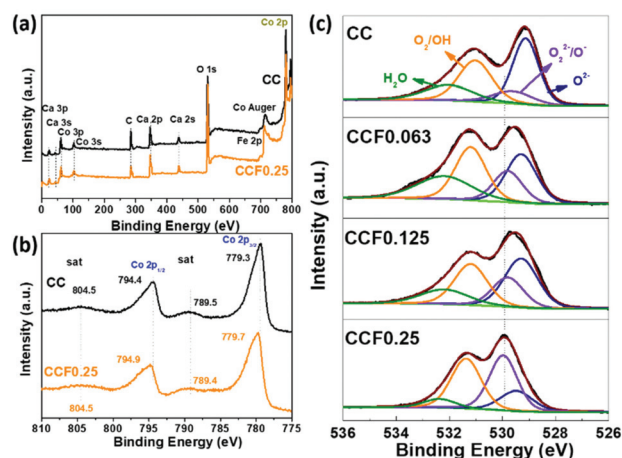


Fig. 6 (a) XPS survey spectra and (b) XPS spectra of Co 2p in CC and CCF0.25. (c) XPS spectra of O 1s species in CC, CCF0.063, CCF0.125 and CCF0.25 nanofibers.

increased in CCF0.25.³⁰ The positive shift of the Co 3p main peak and the decrease of the satellite peak area indicate the oxidation process of Co cations. Moreover, the peaks of both Co 3p and Co 3s show a positive shift and obvious broadening in CCF0.25, which further confirm the partial oxidation of surface Co and the weak splitting of Co, respectively (Fig. S9†). In contrast, the peaks of Fe 2p_{3/2} show a lower binding energy shift (Fig. S10†). It has been reported that cobalt cations with high valence states are beneficial to the OER,^{15,31} as Co with a high valence state facilitates the adsorption and further reaction of OH⁻ to form metal-OOH species,^{15,31} which contributes to the enhanced performance of CCF0.25.

High-resolution O 1s spectra show that all the spectra of CC and CCFx can be split into four well-defined peaks, which correspond with surface-adsorbed molecular water (H₂O, 532.2 eV), adsorbed oxygen or hydroxyl groups (O₂/-OH, 531.2 eV), highly active species (O₂²⁻/O⁻, 529.8 eV) and lattice oxygen species (O²⁻, 529.3 eV) (Fig. 6c).^{31,32} The molar fraction of different oxygen species was evaluated from the relative peak area. The result demonstrates that the area for O₂²⁻/O⁻ species in CCF0.25 (38.9%) is larger than that for CC (11.3%), which could be attributed to the higher OER activity of CCF0.25, as it has been reported that O₂²⁻/O⁻ intermediates produced on the surface of the electrocatalysts are active species for OER.^{33,34} Additionally, with increasing the amount of iron dopant, the relative content of O₂²⁻/O⁻ increased dramatically, which demonstrates the electronic structure regulation after iron doping. The results of the highly reactive oxygen species are in accordance with that in the high-resolution Co spectra.³¹

4. Conclusions

In summary, we have successfully designed a series of layer-structured CC and CCFx nanofibers composed of intercon-

nected ultrathin nanoplates or nanoparticles *via* an electrospinning strategy. By tailoring the nanofiber structure, the surface area has been increased with more active sites exposed. With the introduction of iron dopant in CC, the OER activity of CCFx can be dramatically enhanced. The mass activity and intrinsic activity of CCF0.25 are, respectively, *ca.* 18.7 and 11.4 times higher than those of the original CC at 1.6 V. Among the CC and CCFx nanofibers, the overpotential of CCF0.25 is only 346 mV at 10 mA cm⁻². Iron doping results in the electronic structure change of CC with a partial oxidation of the surface Co and the formation of highly reactive oxygen species (O₂²⁻/O₂). These results not only demonstrate that CCF0.25 is a highly efficient and durable OER electrocatalyst but also pave a promising route for the development of robust OER catalysts with proper doping and tailored nanostructures.

Author contributions

Mingyu Li: Writing – original draft. Bote Zhao: Methodology, conceptualization. Yun Zhao: Investigation, resources. Yu Chen: Validation. Meilin Liu: Supervision.

Conflicts of interest

There are no conflicts to declare.

Acknowledgements

This work was supported by the National Natural Science Foundation of China (52100087, 52102248), the Natural Science Foundation of Chongqing, China (cstc2021jcyj-msxmX0954), and the US National Science Foundation under award number DMR-1742828. M. Y. L. acknowledges the financial support of a scholarship from the China Scholarship Council (CSC).

References

- J. Xu, T. Liu, J. Li, Y. Liu, B. Zhang, D. Xiong, I. Amorim, W. Li and L. Liu, *Energy Environ. Sci.*, 2018, **11**, 1819–1827.
- J. Mahmood, F. Li, S.-M. Jung, M. S. Okyay, I. Ahmad, S.-J. Kim, N. Park, H. Y. Jeong and J.-B. Baek, *Nanotechnol.*, 2017, **12**, 441–446.
- S. Li, Y. Gao, N. Li, L. Ge, X. Bu and P. Feng, *Energy Environ. Sci.*, 2021, **14**, 1897–1927.
- Z. L. Zhao, Q. Wang, X. Huang, Q. Feng, S. Gu, Z. Zhang, H. Xu, L. Zeng, M. Gu and H. Li, *Energy Environ. Sci.*, 2020, **13**, 5143–5151.
- Y. Xiong, Y. Yang, X. Feng, F. J. DiSalvo and H. D. Abruña, *J. Am. Chem. Soc.*, 2019, **141**, 4412–4421.
- H. A. Tahini, X. Tan, U. Schwingschlögl and S. C. Smith, *ACS Catal.*, 2016, **6**, 5565–5570.
- J. Suntivich, K. J. May, H. A. Gasteiger, J. B. Goodenough and Y. Shao-Horn, *Science*, 2011, **334**, 1383–1385.
- L. C. Seitz, C. F. Dickens, K. Nishio, Y. Hikita, J. Montoya, A. Doyle, C. Kirk, A. Vojvodic, H. Y. Hwang, J. K. Nørskov and T. F. Jaramillo, *Science*, 2016, **353**, 1011–1014.
- J. Liu, Y. Ji, J. Nai, X. Niu, Y. Luo, L. Guo and S. Yang, *Energy Environ. Sci.*, 2018, **11**, 1736–1741.
- Q. Ji, C. Li, J. Wang, J. Niu, Y. Gong, Z. Zhang, Q. Fang, Y. Zhang, J. Shi, L. Liao, X. Wu, L. Gu, Z. Liu and Y. Zhang, *Nano Lett.*, 2017, **17**, 4908–4916.
- O. Kasian, S. Geiger, T. Li, J. P. Grote, K. Schweinar, S. Y. Zhang, C. Scheu, D. Raabe, S. Cherevko, B. Gault and K. J. J. Mayrhofer, *Energy Environ. Sci.*, 2019, **12**, 3548–3555.
- H. Zhu, J. Zhang, R. Yanzhang, M. Du, Q. Wang, G. Gao, J. Wu, G. Wu, M. Zhang, B. Liu, J. Yao and X. Zhang, *Adv. Mater.*, 2015, **27**, 4752–4759.
- M. Qin, S. Li, Y. Zhao, C.-Y. Lao, Z. Zhang, L. Liu, F. Fang, H. Wu, B. Jia, Z. Liu, W. Wang, Y. Liu and X. Qu, *Adv. Energy Mater.*, 2019, **9**, 1970003.
- Z. Lu, H. Wang, D. Kong, K. Yan, P.-C. Hsu, G. Zheng, H. Yao, Z. Liang, X. Sun and Y. Cui, *Nat. Commun.*, 2014, **5**, 4345.
- X. Zheng, Y. Chen, X. Zheng, G. Zhao, K. Rui, P. Li, X. Xu, Z. Cheng, S. X. Dou and W. Sun, *Adv. Energy Mater.*, 2019, **9**, 1803482.
- Z. R. Zhang, C. X. Liu, C. Feng, P. F. Gao, Y. L. Liu, F. N. Ren, Y. F. Zhu, C. Cao, W. S. Yan, R. Si, S. M. Zhou and J. Zeng, *Nano Lett.*, 2019, **19**, 8774–8779.
- J. G. Lee, J.-H. Myung, A. B. Naden, O. S. Jeon, Y. G. Shul and J. T. S. Irvine, *Adv. Energy Mater.*, 2020, **10**, 1903693.
- Y. Li, F.-M. Li, X.-Y. Meng, X.-R. Wu, S.-N. Li and Y. Chen, *Nano Energy*, 2018, **54**, 238–250.
- M. Li, Y. Gu, Y. J. Chang, X. C. Gu, J. Q. Tian, X. Wu and L. G. Feng, *Chem. Eng. J.*, 2021, **425**, 130686.
- H. Huang, C. Yu, C. Zhao, X. Han, J. Yang, Z. Liu, S. Li, M. Zhang and J. Qiu, *Nano Energy*, 2017, **34**, 472–480.
- J. Zhou, L. Yuan, J. Wang, L. Song, Y. You, R. Zhou, J. Zhang and J. Xu, *J. Mater. Chem. A*, 2020, **8**, 8113–8120.
- Q. Zhou, Y. Chen, G. Zhao, Y. Lin, Z. Yu, X. Xu, X. Wang, H. K. Liu, W. Sun and S. X. Dou, *ACS Catal.*, 2018, **8**, 5382–5390.
- J. M. P. Martirez and E. A. Carter, *J. Am. Chem. Soc.*, 2019, **141**, 693–705.
- S. Zhang, B. Huang, L. Wang, X. Zhang, H. Zhu, X. Zhu, J. Li, S. Guo and E. Wang, *ACS Appl. Mater. Interfaces*, 2020, **12**, 40220–40228.
- M.-Q. Wang, C. Ye, H. Liu, M. Xu and S.-J. Bao, *Angew. Chem., Int. Ed.*, 2018, **57**, 1963–1967.
- B. Zhao, L. Zhang, D. Zhen, S. Yoo, Y. Ding, D. Chen, Y. Chen, Q. Zhang, B. Doyle, X. Xiong and M. Liu, *Nat. Commun.*, 2017, **8**, 14586.
- C. Lv, J. Sun, G. Chen, Y. Zhou, D. Li, Z. Wang and B. Zhao, *Appl. Catal., B*, 2017, **208**, 14–21.
- Y. L. Zhu, W. Zhou, Z. G. Chen, Y. B. Chen, C. Su, M. O. Tade and Z. P. Shao, *Angew. Chem., Int. Ed.*, 2015, **54**, 3897–3901.

- 29 S. Zhou, X. Miao, X. Zhao, C. Ma, Y. Qiu, Z. Hu, J. Zhao, L. Shi and J. Zeng, *Nat. Commun.*, 2016, **7**, 11510.
- 30 X. Han, C. Yu, S. Zhou, C. Zhao, H. Huang, J. Yang, Z. Liu, J. Zhao and J. Qiu, *Adv. Energy Mater.*, 2017, **7**, 1602148.
- 31 Y. Zhu, W. Zhou, Y. Chen, J. Yu, M. Liu and Z. Shao, *Adv. Mater.*, 2015, **27**, 7150–7155.
- 32 J. Dai, Y. Zhu, Y. Chen, W. Zhou and Z. Shao, *ACS Appl. Mater. Interfaces*, 2017, **9**, 21587–21592.
- 33 R. Liu, F. Liang, W. Zhou, Y. Yang and Z. Zhu, *Nano Energy*, 2015, **12**, 115–122.
- 34 J. I. Jung, H. Y. Jeong, J. S. Lee, M. G. Kim and J. Cho, *Angew. Chem., Int. Ed.*, 2014, **53**, 4582–4586.